Int. J. Electrochem. Sci., 7 **(2012)** 5746 - 5753

International Journal of
ELECTROCHEMICAL
SCIENCE
www.electrochemsci.org

Double-barrier Superlattice Infrared Photodetector Integrated with Multiple Quantum-Well Infrared Photodetector to Improve Performance

Shih-Hung Lin[1], *David Jui-Yang Feng*[2], *Ming-Lun Lee*[1], *Tsong-Sheng Lay*[3], *Tai-Ping Sun*[4], *Chieh-Hsiung Kuan*[1,*]

[1] Department of Electrical Engineering and Graduate Institute of Electronics Engineering, National Taiwan University, Taipei 10617, Taiwan,
[2] Department of Electrical Engineering, National University of Kaohsiung, Kaohsiung 804, Taiwan,
[3] Department of Photonics and Institute of Electro-Optical Engineering, National Sun Yat-Sen University, Kaohsiung 804, Taiwan
[4] Department of Electrical Engineering, National Chi-Nan University, Puli 545, Taiwan,
[*]E-mail: kuan@cc.ee.ntu.edu.tw

Received: 13 February 2012 / *Accepted:* 17 March 2012 / *Published:* 1 July 2012

An infrared photodetector which has a 15-period superlattice (SL) sandwiched by double barriers with multiple quantum wells (MQWs) inserted in the right side of them has investigated. Photoelectrons can bounce back and forth in the second miniband between two barriers and then inject through the graded barrier to enhance the photocurrent. MQWs is utilized to reduce the noise current power and add response range. Because of enhanced photocurrent and low noise gain, this detector shows satisfactory detectivity (D*) 1.85×10^{10} cm $Hz^{0.5}$/W (at 8.2 μm and 0.7 V under 80 K). Due to combination of superlattice and multiple quantum wells infrared photodetectors, multi-color detection can be achieved by bias magnitude modification. From the experimental results, this device is the promising candidate of a pixel in the focal plane array.

Keywords: Superlattice, photodetector, Infrared

1. INTRODUCTION

Much effort has been devoted in seeking the infrared photodetectors operated under high temperature and at low bias with optimized performance for a pixel in the focal plane array (FPA) [1 - 6]. To fabricate the quantum-well infrared photodetectors (QWIPs)-based FPA, the high current density and capacitor saturation of readout IC (ROIC) should be avoided. Thus, the device may operate

under low bias to lower dark current density but the associated low photoresponse should be improved. In comparison with quantum-well infrared photodetectors (QWIPs), the advantages of superlattice infrared photodetectors (SLIPs) are voltage tunability, low-voltage operation, and broadband photoresponse [7-8]. In general, the structure of a conventional SLIP is period of superlattice integrated with a single barrier. The functions of the single barrier are to be a bias-tuned energy filter and to reduce the dark current [7-9]. However, the primary drawback of SLIPs is low responsibility. The SLIPs with improvement of the responsivity and decrement of noise under low bias in order to increase final detectivity is main purpose for FPA system.

In this paper, we utilize superlattice (SL) and multiple quantum well (MQW) as active regions to achieve multi-color detection. The thick and graded barriers are used for photoelectrons to resonate in the second miniband of SL to increase photoelectrons tunneling probability. The MQWs are acted as noise filter to reduce the noise power and therefore improve device's performance. These designs make this device achieve this purpose.

2. EXPERIMENTAL PROCEDURE

The sample layers from bottom to top are an emitter layer (Bottom contact), a 500 nm $Al_{0.33}Ga_{0.67}As$ thick blocking barrier, a 15-period SL (superlattice contact), a graded barrier $Al_xGa_{1-x}As$ (X=0.29-0.21), a 30-period MQWs and a collector layer (Top contact). Each period of the SL (QW) consists of 6.5 (5) nm GaAs well with 4×10^{17} cm^{-3} Si donors and 3.5 nm $Al_{0.32}Ga_{0.68}As$ barrier undoped (60 nm $Al_{0.21}Ga_{0.79}As$ barrier undoped). The absorption wavelength of the SL is from 6 to 12 μm.

Two detectors were farbricated from the same sample but with different mesas. Detector 1 was processed to form the 100 μm × 100 μm square mesas and etched down to the emitter layer, then evaporated Au/Ge/Ni (70 nm Ni/Ge/Au and 230 nm Au) onto the top of each mesa as the collector (Top) and also the bottom as the emitter (Bottom). However, Detectors 2 is etched down only to the middle superlattice layer (Fig. 1) then evaporated Au/Ge/Ni onto SL to form the superlattice contact.

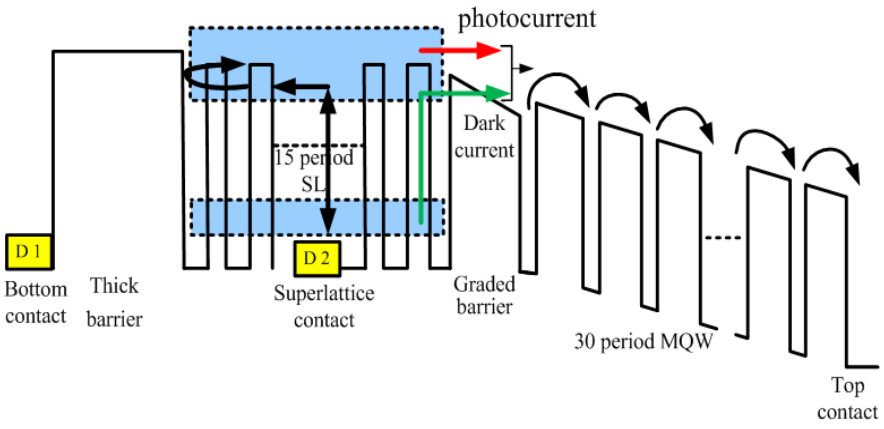

Figure 1. Schematic energy band diagram of Detector 1 (D1) and 2 (D2), a thick barrier, 15-period SL, graded barrier and MQWs under low bias. The red and green arrows indicate photocurrent and dark current respectively.

A 45^{o} facet on the sample substrate is fabricated to allow the TM polarized infrared light to radiate on the photodetector. The positive bias is defined as the top contact layer is positive. The spectral response of a detector can be measured by a monochromator and a blackbody IR source, or a Fourier transform IR (FTIR) system. In our experiments, we use Perkin Elmer 2000 as the FTIR to measure the spectral response. Fig. 2 shows the setup of the measurement of spectral response. Devices are mounted on a closed-cycle cryostat system. Devices' photocurrent generated by the infrared source in FTIR is first amplified and converted to voltage signal by a low noise current preamplifier (Stanford Research SR570), and then input to the FTIR. The interference intensity is therefore transformed by the built-in program in FTIR to obtain the spectrum. A spectrally flat detector is used to normalize the system spectral response due to the wavelength dependence. The absolute magnitude of the responsivity is then determined by the photocurrent with a calibrated blackbody source.

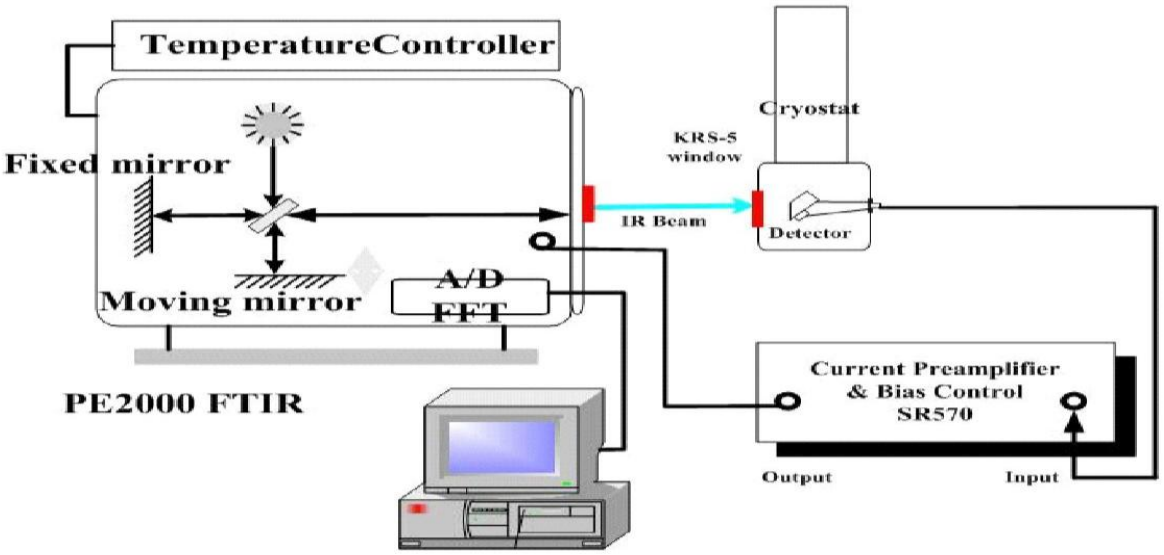

Figure 2. The setup of the measurement of photoresponse.

3. RESULTS AND DISCUSSION

We will show and compare these detectors' performances such as current-voltage (*I-V*) characteristics, spectral responsivity and detectivity. Then, we will discuss the physical mechanisms which result in the difference performance between these detectors.

3.1. I-V Characteristics

Fig. 3 (a) and (b) present the dark current at different temperatures and 20K photocurrent under 300 K background radiation of Detector 1, and 2, respectively. We can observe that the I-V

relationship in Detector 1 is asymmetric, while that in Detector 2 is quite symmetric with respect to the bias. [8–11] Background limited infrared performance (BLIP) of Detector 1 is about 40 K under the bias range from 0–4 V with bias applied between top and bottom contacts. It is noted that the background photocurrent is above 80 K dark current of Detector 2 from 0–4 V with bias applied between top and superlattice contacts. The inset of Fig. 3 (a) shows I-V curve of Detector 2 under ultra low bias in detail.

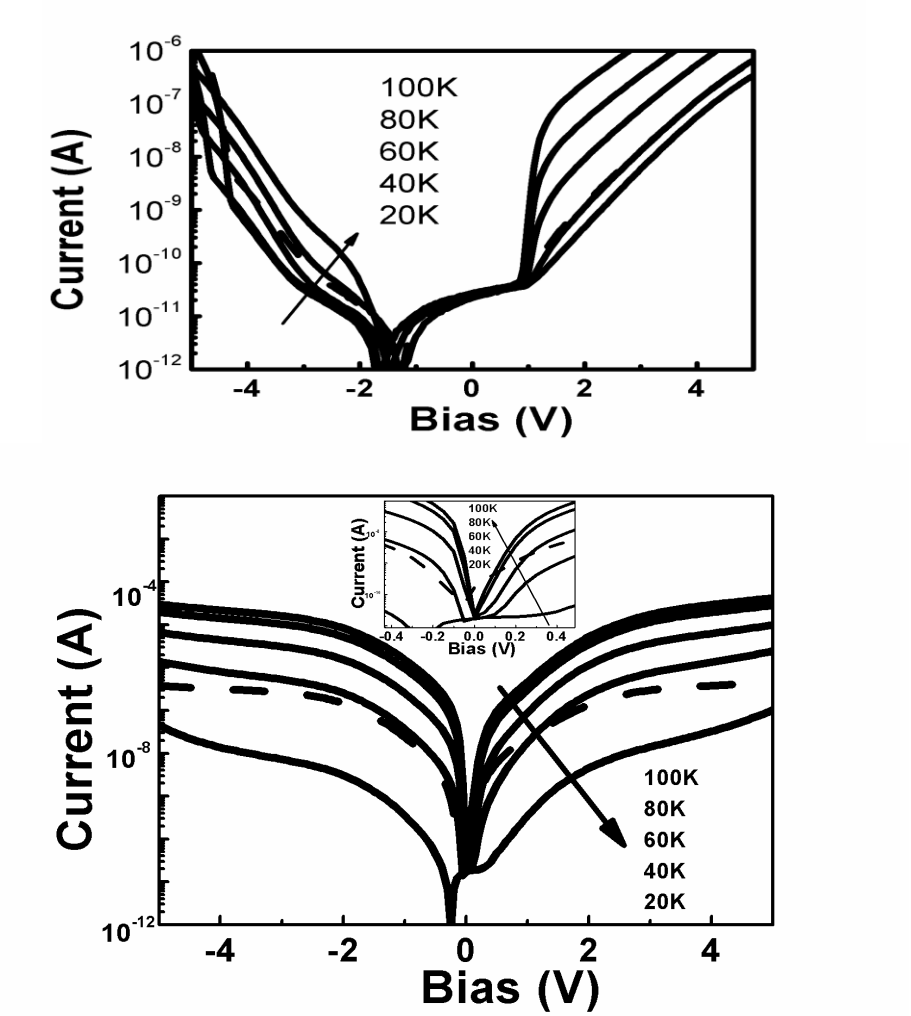

Figure 3. (a) The dark current (solid lines) at different temperatures and the photocurrent at 20 K (dashed line) versus the bias of Detector 1. (b) I-V curves of Detector 2 at the same condition. Inset of (b) is the dark current (solid lines) at different temperatures and the photocurrent at 20 K (dashed line) of Detector 2 versus the bias voltage under very low bias.

3.2. Photoresponse

To further demonstrate the photocurrent improvement of Detector 2, the spectral responsivity of two detectors is measured. Figure 4 and 5 show the spectral responsivity versus wavelength for Detector 1 under bias ranges of 3.0–4.0 V at 80 K, and Detector 2 under 0.3–0.11 V at 80 K. The 8.2 μm peak can be observed clearly, but 10.3 μm peak is very weak under low bias (multi-color detection

is not obvious). Detector 2 shows multi-color detection at 8.2 μm from SLIP and 10.3 μm from QWIP under different bias at 80 K. The bias range is about 0.3–1.1V for both peak and the responsivity of 8.2 μm is quiet larger than 10.3 μm. However, the 10.3 μm peak disappeared at 90 K (inset of Fig. 5) due to high dark current magnitude of QWIP under high temperature [8]. Responsivity of Detector 2 at 80 K is much higher than Detector 1 at 80 K. It is noted that Responsivity of Detector 2 at 90 K is still higher than that of Detector 1 at 80 K.

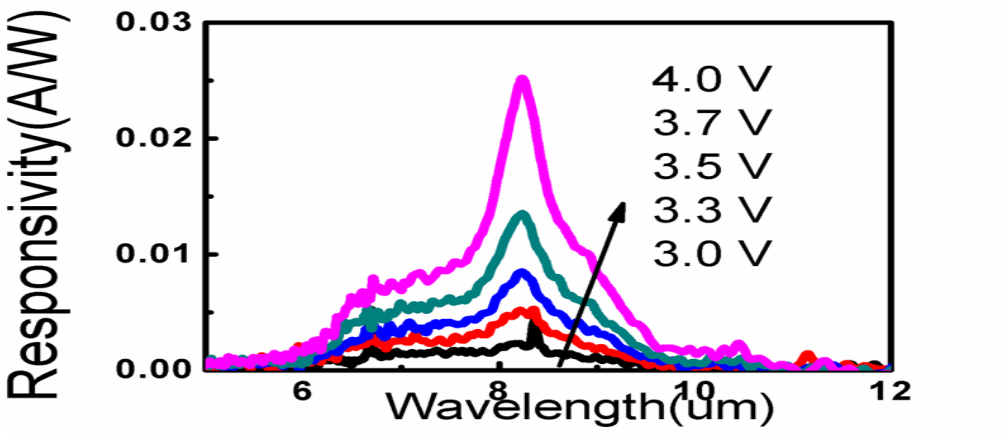

Figure 4. The spectral responsivity versus wavelength at 80 K of Detector 1 with bias range of 3.0–4.0 V.

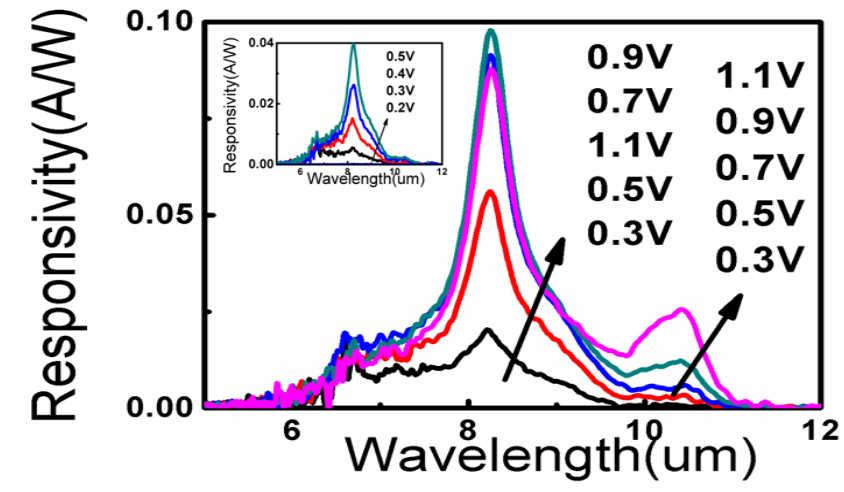

Figure 5. The spectral responsivity versus wavelength of Detector 2 with bias range of 0.3–1.1 V, and the inset shows that at 90K at 0.2–0.5V.

3.3. Detectivity

From the experimental results of responsivity and dark current, the detectivity (D*) at different bias and 80K for Detector 1 at 80 K (upper axis) and Detector 2 at 80 K and 90 K (lower axis) are calculated (Fig. 6). Here, we choose D* at 8.2 μm which comes from SLIP structure and compare it

between Detector 1 and 2. The maximum detectivity value of Detector 2 (at 0.7 V and 80 K) is 1.85 × 10^{10} cm $Hz^{0.5}$/W which is higher than that of Detector 1 at 80 K and previous works [8-10, 12-14]. It is worthy to mention that the maximum detectivity of Detector 2 at 90 K is also higher than that of Detector 1 at 80 K at very low bias due to higher responsivity and lower dark current.

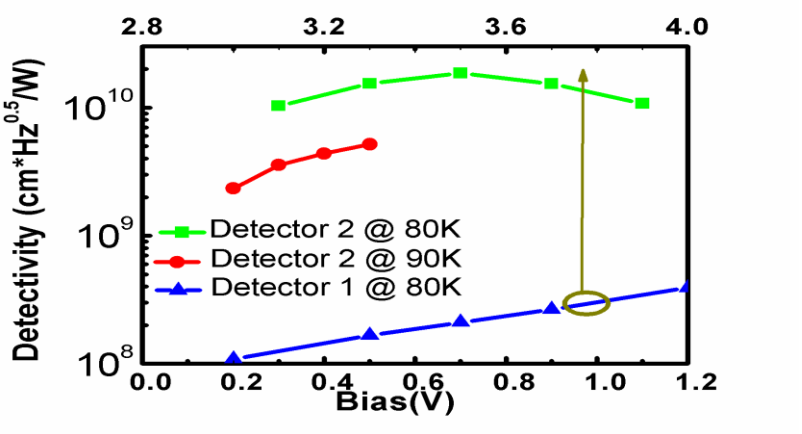

Figure 6. Detectivity (D*) of Detector 1 at 80 K (upper axis) and Detector 2 at 80 and 90 K (lower axis) versus positive bias. (corresponding D* wavelength is 8.2 μm)

3.4. Discussions

Due to thick barrier of this structure, the difficult supplement of electrons from the emitter through thick barrier would result in charge supply limitation in SL layer in Detector 1. So the I-V curve of Detector 1 would be asymmetry. To avoid this problem, Detectors 2 is fabricated by etching down only to the SL active region and SL contact can support and supply carriers easily (The bias is applied between the top and SL contacts). From Fig. 3(a) and (b), we can observe I-V curve of Detector 2 is very symmetry and higher BLIP than Detector 1. Because etching down only to the SL in Detector 1, charge supply limitation problem can overcome [8-11].

After solving charge supply limitation problem, we further study responsivity improvement by comparing Fig. 4 with Fig. 5. In Detector 2, the photoelectrons excited from first miniband to second miniband can resonate in second miniband between thick and graded barriers to increase tunneling probability. The simulation and experimental proof can refer to our previous work [8-9]. In addition to the photocurrent enhancement, the noise reduction is also critical to improve device's final performance. In general, the SL is integrated with a single barrier to reduce the dark current. In this work, we replace a single barrier by MQWs. For a SL with a single barrier, the noise is thermally assisted tunneling (TAT) and is given by the shot noise performance [10, 12–13] as:

$$i_{SB}^2 = 2eI_D$$

where i_{SB} is the noise current power spectral density (PSD) of this structure and ID is its dark current.

The noise in MQWs is the generation-recombination noise and is given by

$$i_{QW}^2 = 4eg_n I_D,$$

where i_{QW} is the noise current PSD of MQWs, gn is the noise gain of MQWs and I_D is dark current of MQWs, so MQWs can be utilized as noise filter if g_n can be much less than 1 at low biases. Almost all electrons traversing a barrier are recaptured into the neighboring well and produce the capture current because of the high capture probability under low bias. Under steady state, capture current must be balanced by the emission current. This capture and emission process will repeat till the last quantum well (Fig. 1). The photocurrent of SL is not reduced by MQWs but associated noise power is. Therefore, this device is expected to operate at low bias. Due to combination of enhancement of photocurrent and reduction of dark current, detectivity of Detector 2 at 80 and 90 K are higher than that of Detector 1 at 80 K (Fig. 6).

Multi-color detection can be also realized in this detector by bias maginitude modification due to combination of SL and MQWs. Under high bias, the dark current in MQWs is too high and therefore we can not obtain 10.3 μm at 80K. In the contrast, both 8.2 μm (from SL) and 10.3 μm (from MQWs) can be observed in Detector 2 at 80 K under low bias. With temperature exceeding 90 K, 10.3 μm peak disappeared due to very high dark current for MQWs at high temperature (Fig. 5). Therefore, SL is suit for high temperature operation. [14]

4. CONCLUSION

We have investigated and study a double barrier superlattice infrared photodetector integrated with multiple quantum well infrared photodetector. In this detector, photoelectrons can resonate in the second miniband between thick and graded barriers to enhance the photocurrent. The function of MQWs is to reduce the noise current power and add response range. Therefore, performance of this detector is improved than our previous work. This detector also shows two well-defined peaks covering 6-12 μm, and the associated detectivity at high temperature is satisfactory. The improvement of such kind SLIP makes it be promising candidate of a pixel in the focal plane array. However, the tradeoff is the small operation voltage range.

ACKNOWLEDGEMENTS
This work was supported by National Science Council of Taiwan, under Contract NSC 100-2221 E-390-017 and NSC 97-2221-E-002-053-MY3, NTU center for information and electronics technology 10-R-80919 and 10-R-80300, and NTU 100-C-1337.

References

1. S. Ozer, O. O. Cellek and C. Besikci," *Infra. Phys. & Technol*. 47 (2005) 115
2. E. Costard, Ph. Bois, X. Marcadet and A. Nedelcu, *Infra. Phys. & Technol.* 47 (2005) 115.

3. S. D. Gunapala, S. V. Bandara, J. K. Liu, C. J. Hill, S. B. Rafol, and J. M. Mumolo," *IEEE Trans. Electron. Dev.* 50 (2003) 2353
4. B. F. Levine, "Quantum-well infrared photodetector," *J. Appl. Phys.* 74 (1993) 1
5. H. Schneider, T. Maier, J. Fleissner, M. Walther, P. Koidl, G. Weimann, W. Cabanski, M. Finck, P. Menger, W. Rode, and J. Ziegler, *Infra. Phys. & Technol.* 47 (2005) 53
6. C. S. Wu, C. P. Wen, P. Reiner, C. W. Tu and H. Q. Hou, *Solid State Electron*. 39 (1996) 1253
7. M. C. Hsu, Y. F. Hsu, S. Y. Lin and C. H. Kuan, *IEEE Trans. Electron Dev.* 47 (2000) 944
8. S. H. Lin, J. Y. Feng, J.H. Lu, T. S. Lay, C. H. Kuan , *J. Electrochemical Soc*.158 (2011) H370
9. S. H. Lin, Y. H. Wang, C. W. Chang, J. H. Lu, C. C. Chen, and C. H. Kuan, *Cutting Edge Nanotechnology*, p. 121, In-Tech, Croatia (2010).
10. J. H. Lu, K. J. Wu, K. J. Hsieh, C. H. Kuan, C. W. Yang, S. L. Tu, J. Y. Feng and T. S. Lay, *IEEE J. Quant. Electron* 43 (2007) 72
11. S. F. Tang, S. Y. Lin and S. C. Lee, *IEEE Trans. Electron Dev.* 49 (2002) 1341
12. J. H. Lu, Y. Y. Yang, C. C. Chen, C. H. Kuan, H. D. Chen and S. C. Lee, *Infra. Phys. & Technol.*44 (2003) 399
13. J. H. Lu, Y. C. Wang, C. L. Wang, C. H. Kuan, C. W. Yang, S. L. Tu, J. Y. Feng,and T. S. Lay, *J. Appl. Phys.* 102 (2007) 074542
14. C. C. Chen, H. C. Chen, M. C. Hsu, W. H. Hsieh, C. H. Kuan, S. Y. Wang and C. P. Lee *J. Appl. Phys.* 91 (2003) 943